Dalton Transactions

PAPER

View Article Online
View Journal | View Issue

Cite this: *Dalton Trans.*, 2017, **46**, 5965

Variable coordination of tris(2-pyridyl)phosphine and its oxide toward $M(hfac)_2$: a metal-specifiable switching between the formation of mono- and bis-scorpionate complexes†

Alexander V. Artem'ev,* [a] Alexey V. Kashevskii,[b] Artem S. Bogomyakov,[c] Alexander Yu. Safronov,[b] Anastasiya O. Sutyrina,[d] Anton A. Telezhkin[d] and Irina V. Sterkhova[d]

An unexpected substitution of the anionic chelating ligands at the M^{II} centre by a neutral tripodal ligand has been observed in the reaction of Mn^{II}, Co^{II}, Ni^{II} and Cu^{II} hexafluoroacetylacetonates (hfac) with tris(2-pyridyl)phosphine (Py_3P) or its oxide (Py_3P = O). The nature of the metal ion in $M(hfac)_2$ and the M/L ratio determine the degree of substitution of hfac-anions (partial *vs.* total) and therefore, the structure of the complex formed (scorpionate *vs.* bis-scorpionate ones, respectively). Hence, the reaction of the ligands with $[Cu(hfac)_2(H_2O)_2]$ in an equimolar ratio affords scorpionate $[Cu(N,N',N''\text{-}Py_3P = X)(O,O'\text{-hfac})(O\text{-hfac})]$, wherein one hfac-ligand chelates metal, while the other hfac acts as an *O*-monodentate one. Using the two equivalents of Py_3P in this reaction leads to $[Cu(N,N',N''\text{-}Py_3P)_2](hfac)_2$, which contains a bis-scorpionate cation $[Cu(Py_3P)_2]^{2+}$ and two noncoordinated hfac-anions. $[Co(hfac)_2(H_2O)_2]$ and $[Ni(hfac)_2(H_2O)_2]$, regardless of the M/L molar ratio, react with Py_3P = O to give cationic scorpionates $[M(N,N',N''\text{-}Py_3P = O)(O,O'\text{-hfac})(H_2O)](hfac)$, in which one hfac-anion is noncoordinated. In contrast, $[Mn(hfac)_2(H_2O)_2]$, on interaction with Py_3P, results in the cationic complex $[Mn(N,N',N''\text{-}Py_3P)_2][Mn(hfac)_3]_2$ bearing a bis-scorpionate cation $[Mn(Py_3P)_2]^{2+}$ and two $[Mn(hfac)_3]_2^-$ counterions. The synthesized scorpionates have been characterized by X-ray diffractometry, cyclic voltammetry, SQUID magnetometry, FT-IR and UV-Vis techniques.

Received 28th January 2017,
Accepted 1st April 2017

DOI: 10.1039/c7dt00339k

rsc.li/dalton

1. Introduction

During the past decades, pyridylphosphines and their chalcogenides have attracted increasing attention in coordination chemistry, catalysis and material science.[1–3] The combination of "soft" (P-atom) and "hard" (N-atoms) donor sites in pyridylphosphines makes them very important and versatile ligands for the design of unique catalysts,[4] luminescent materials[5] and prospective drugs.[6] Among pyridylphosphines, tris(2-pyridyl)phosphine (Py_3P) is gaining a special interest owing to the useful properties of its metal complexes. For instance, Pd,[7,8] Cr,[9] Mo,[9] W,[9,10] Ru[11] and Rh,[11] Fe,[12] Co,[12,13] Ni[13] and Mn[13] complexes with Py_3P have been explored as catalysts for methoxycarbonylation of alkynes,[7,8] Diels–Alder cycloaddition,[9] Friedel–Crafts/aldehyde cyclotrimerization,[10] hydroformylation of alkenes,[11] ethylene polymerization,[12] and O_2-oxidation of tetraline.[13] Most significantly, Py_3P has recently become readily available due to the development of its synthesis directly from elemental phosphorus and 2-bromopyridine.[14]

Tris(2-pyridyl)phosphine, owing to its tripodal structure and heminal disposition of the N atoms towards the P atom, exhibits numerous coordination patterns, *e.g.* *N*-[15] and *P*-monodentate,[14,16] *P*,*N*-bridging,[17] *N*,*N*′-chelating,[18,19] *N*,*P*,*N*′-pincer,[20] *N*,*N*′/*P*-bridging[21] and *N*,*N*′,*N*″-tripodal[9,22–24] ones. A while ago, *N*,*N*′,*N*″-/*P*-coordination of substituted tris(2-pyridyl)phosphine was found in the dinuclear complex $[(MeCN)_3Cu\{P(6\text{-Me-2-Py})_3\}Cu(MeCN)](PF_6)_2$, wherein this ligand acts as a Janus head ligand.[25]

In contrast to the plethora of studies related to tris(2-pyridyl)phosphine based complexes, the data on those with

[a]*Nikolaev Institute of Inorganic Chemistry, Siberian Branch of Russian Academy of Sciences, 3, Akad. Lavrentiev Ave., Novosibirsk 630090, Russian Federation. E-mail: chemisufarm@yandex.ru*
[b]*Irkutsk State University, Karl Marx str., 1, 664003 Irkutsk, Russian Federation*
[c]*International Tomography Center, SB RAS, Institutskaya Str. 3A, 630090 Novosibirsk, Russian Federation*
[d]*A. E. Favorsky Irkutsk Institute of Chemistry, Siberian Branch of the Russian Academy of Sciences, 1 Favorsky Str., 664033 Irkutsk, Russian Federation*

†Electronic supplementary information (ESI) available: Copies of FT-IR, excitation and emission spectra; computation details. CCDC 1431158, 1431160, 1431159, 1033904, 1036445 and 1035512. For ESI and crystallographic data in CIF or other electronic format see DOI: 10.1039/c7dt00339k

tris(2-pyridyl)phosphine chalcogenides, $Py_3P = X$ (X = O, S or Se), are scarce, although the latter are equally important ligands. In recent years, these complexes have been employed for the synthesis of the scorpionate complexes [Cu(*N*,*N*′,*N*″-$Py_3P = X$)]Hal,[26,27] showing yellow to red TADF emission with good quantum yields.[27] Later, a series of Cu^I thiocyanate complexes with $Py_3P = O$ was designed.[28] The Ru^{II} scorpionate supported by the $Py_3P = O$, *viz.* [Ru(*N*,*N*′,*N*″-$Py_3P = O$)(bpy)(OH_2)]$(OTf)_2$, has proven to be an excellent electrocatalyst for water oxidation, thus surpassing any known Ru catalyst.[29]

Therefore, the further development of the coordination chemistry of tris(2-pyridyl)phosphine and its chalcogenides appears to be particularly appealing to access novel functional compounds. Herein, as a part of our ongoing interest in this area, we report on the variable coordination of tris(2-pyridyl) phosphine (**1**) and its oxide (**2**) towards $M(hfac)_2$ (M = Cu, Ni, Co, Mn) leading to either scorpionate or bis-scorpionate complexes. In the course of this study, we have observed an unexpected replacement of the anionic chelating ligand at the metal center by the neutral tripodal ligand. The degree of such substitution (partial *vs.* complete) and, hence, the structure of the resulting complexes (scorpionate *vs.* bis-scorpionate) depend on the nature of the metal ion in $M(hfac)_2$ and, to a lesser extent, on a metal-to-ligand ratio.

2. Results and discussion

2.1. Synthetic aspects

As our experiments have shown, the reaction of [Cu$(hfac)_2(H_2O)_2$] with Py_3P (**1**) at the 1 : 1 molar ratio occurs immediately upon mixing of the reactants ($CHCl_3$, r.t.) to give scorpionate **3** in 88% yield (Scheme 1). The reaction is strictly selective: a possible formation of the coordination polymers does not take place. In the structure of **3**, Py_3P acts as *N*,*N*′,*N*″-tripodal ligand toward the octahedral Cu^{II} ion. Importantly, during the reaction, one of the hfac-anions retains an *O*,*O*′-chelating pattern, whereas the second hfac-anion adopts an *O*-monodentate mode. The reaction of $Py_3P = O$ (**2**) with [Cu$(hfac)_2(H_2O)_2$] under similar conditions (1 : 1 ratio, r.t., $CHCl_3$) instantly leads to structurally related scorpionate **4** in 80% yield (Scheme 1). Therefore, the charge of the P atom in **1** and **2** (δ− *vs.* δ+, respectively) has no influence on the result of the reaction with $Cu(hfac)_2$. This can be explained by weak or a complete lack of conjugation between the phosphorus-centered orbitals and the π-electronic system of the pyridine rings.

Moreover, the interaction of [Cu$(hfac)_2(H_2O)_2$] with Py_3P in a 1 : 2 ratio at ambient temperature ($CHCl_3$ or MeCN) produces complex **5** in 78% yield (Scheme 1). Thus, both chelating hfac-anions within the coordination sphere of Cu^{II} are replaced by the Py_3P ligands. In the complex obtained (**5**), the Cu^{II} ion octahedrally coordinates six N atoms of two Py_3P molecules to form a bis-scorpionate cation $[Cu(Py_3P)_2]^{2+}$. The two hfac-anions are in the second coordination sphere.

Notably, $Cu(acac)_2$ does not react with Py_3P or $Py_3P = O$; after removing the solvent from the reaction mixture, the starting reagents remain unchanged. The observed discrepancy is likely due to a higher Lewis acidity of Cu^{II} in $Cu(hfac)_2$ caused by the presence of two strong electron-acceptor hfac-ligands.

To our surprise, the reaction between $Py_3P = O$ and [Co$(hfac)_2(H_2O)_2$] or [Ni$(hfac)_2(H_2O)_2$], regardless of the M/L molar ratio, always furnishes scorpionates **6** or **7** in 85% and 81% yields, respectively (Scheme 2). Importantly, unlike **3** and **4**, in the scorpionates **6** and **7**, the M^{II} ion of the {M(*N*,*N*′,*N*″-$Py_3P = O$)} unit is coordinated by one chelating hfac-anion and H_2O molecule, thus adopting an octahedral geometry, while another hfac-ligand is noncoordinated. Our attempts to synthesize bis-scorpionate Co^{II} and Ni^{II} complexes by the reaction of [M$(hfac)_2(H_2O)_2$] with excess **2** were unsuccessful; only complexes **6** and **7** were obtained along with unreacted ligand. In contrast, when $Co(NO_3)_2{\cdot}7H_2O$,[23] $CoCl_2{\cdot}6H_2O$[30] and $NiCl_2{\cdot}6H_2O$,[31] react with Py_3P in 1 : 2 molar ratio, bis-scorpionate complexes of $[M(Py_3P)_2]^{2+}$ type are readily formed.

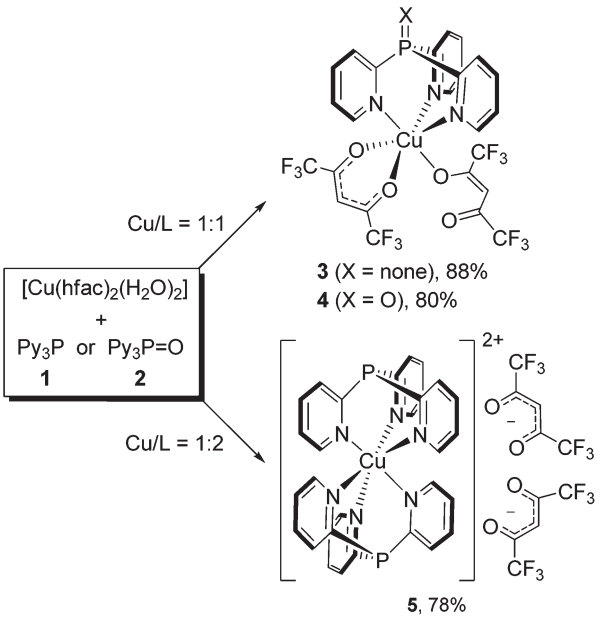

Scheme 1 Synthesis of mono- and bis-scorpionate complexes **3**–**5**.

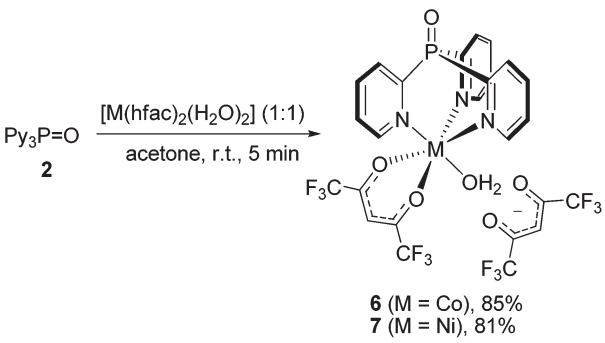

Scheme 2 Synthesis of scorpionate complexes **6** and **7**.

Surprisingly, the treatment of $[Mn(hfac)_2(H_2O)_2]$ with Py_3P in 1 : 1 or 1 : 2 molar ratio (r.t., MeCN) immediately produces complex $[Mn(N,N',N''\text{-}Py_3P)_2][Mn(hfac)_3]_2$ (**8**), as shown in Scheme 3. Using a stoichiometric ratio of the reactants (3 : 2) affords **8** in 69% yield. In the bis-scorpionate $[Mn(Py_3P)_2]^{2+}$ cation, the metal has an octahedral environment arranged from six N atoms of two Py_3P ligands. In the crystal of **8**, there are two stereochemically different $[Mn(hfac)_3]^-$ anions (Δ- and Λ-isomers), in which the Mn^{II} coordinates three hfac-anions to form a MnO_6 twisted prism.

These results suggest that the outcome of the reaction between $M(hfac)_2$ and Py_3P or Py_3P = O is strongly influenced by the nature of M^{II} ions and, in the case of $Cu(hfac)_2$, by the M/L ratio specified. In the reaction with $Cu(hfac)_2$, the final product may be the scorpionate (**3** or **4**) or bis-scorpionate (**5**) complex, whilst $Co(hfac)_2$ and $Ni(hfac)_2$ give only mono-scorpionates (**6** and **7**). Unlike these, $Mn(hfac)_2$ interacts with **1**, furnishing the unexpected complex $[Mn(N,N',N''\text{-}Py_3P)_2][Mn(hfac)_3]_2$ (**8**). Therefore, in the reactions investigated, the replacement of the charged chelating ligands by the neutral tripodal ligands is observed. When $M(acac)_2$ (exemplified by Cu^{II} acetylacetonate), is used as the starting reagent, no reaction with the Py_3P or Py_3P = O is observed. The different behavior of $M(acac)_2$ and their polyfluorinated analogues is probably due to the better leaving group ability of the hfac-anion compared with that of the acac-anion.

The observed that the difference in reactivity of $M(hfac)_2$ toward Py_3P or Py_3P = O can be rationalized by the interference of two factors. First, it is well known[32] that within a series of octahedral complexes, the lability toward ligand substitution generally increases in the sequence: Cu^{2+} $[t_{2g}^{(6)}e_g^{(3)}]$ > Mn^{2+} $[t_{2g}^{(3)}e_g^{(2)}]$ > Co^{2+} $[t_{2g}^{(5)}e_g^{(2)}]$ > Ni^{2+} $[t_{2g}^{(6)}e_g^{(2)}]$ due to the filling of the t_{2g} and e_g orbitals. Therefore, $[Cu(hfac)_2(H_2O)_2]$ and $[Mn(hfac)_2(H_2O)_2]$ are expected to be more substitutionally labile compared to $[Co(hfac)_2(H_2O)_2]$ and $[Ni(hfac)_2(H_2O)_2]$, which agrees with the complete replacement of both hfac-ligands in Cu^{II} and Mn^{II} precursors. On the other hand, the interaction of lesser labile $[Co(hfac)_2(H_2O)_2]$ and $[Ni(hfac)_2(H_2O)_2]$ with Py_3P = O, regardless of their ratio, always gives scorpionates **6** and **7**, wherein the parent hfac-anion and water molecule remain coordinated to the metal. In contrast, $[Cu(hfac)_2(H_2O)_2]$, when reacted with Py_3P or Py_3P = O in a 1 : 1 ratio, forms scorpionates **3** and **4**, in which the metal is coordinated by chelating and monodentate hfac-anions. In other words, the total substitution of the two H_2O molecules and partial substitution of a hfac-ligand within $[Cu(hfac)_2(H_2O)_2]$ takes place in this reaction. The possible explanation of this fact is that the $[Cu(hfac)_2(H_2O)_2]$, being subjected to a Jahn–Teller distortion,[33] features a faster substitution of axially located H_2O molecules compared to the equatorial hfac-anions. Furthermore, the lower reactivity of $[Co(hfac)_2(H_2O)_2]$ and $[Ni(hfac)_2(H_2O)_2]$, for which the partial substitution of hfac-anions is observed, is consistent with maximum charge density (Z^2/r) at the Co^{2+} or Ni^{2+} ion (5.37 and 5.79)[34] compared with the value for Mn^{2+} (4.82).[34] As a consequence, the breaking of the metal–O_{hfac} and metal–O_{H_2O} bonds in $[Co(hfac)_2(H_2O)_2]$ and $[Ni(hfac)_2(H_2O)_2]$ as well as in the resulting complexes **6** and **7** becomes more difficult.

The synthesized complexes are air-stable crystals, which are well soluble in MeCN, Me_2CO and $CHCl_3$. Moreover, complex **8** is soluble in Et_2O and, partially, in hexane. In the solid state, complexes **3–8** have been characterized by X-ray diffraction analysis (the crystallographic data are given in Table S1†), SQUID magnetometry and ATR-IR spectroscopy, while their redox behaviour has been studied using cyclic voltammetry (CV).

2.2. Crystal structure description

In scorpionate **3** (Fig. 1), the Cu atom has a 4 + 2 pseudooctahedral environment, where the equatorial plane is defined by

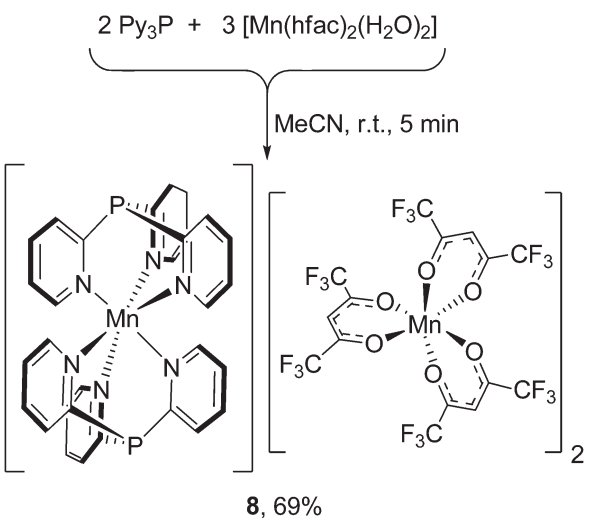

Scheme 3 Synthesis of bis-scorpionate complex **8**.

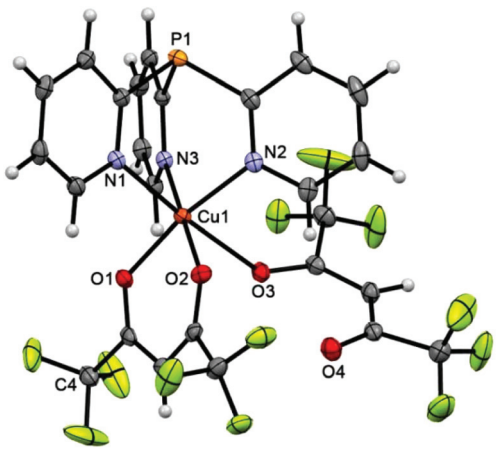

Fig. 1 Molecular structure of **3** (50% thermal ellipsoid). The minor disorder of the CF_3 (C4) group is omitted for clarity. Selected bond lengths [Å] and angles [°]: Cu(1)–O(1) 1.9729(11), Cu(1)–O(2) 1.9867(12), Cu(1)–O(3) 2.474(10), Cu(1)–N(2) 2.0101(13), Cu(1)–N(3) 2.0152(13), Cu(1)–N(1) 2.2575(14), N(1)–Cu(1)–O(3) 175.87, O(2)–Cu(1)–N(3) 177.78(5), O(1)–Cu(1)–N(2) 169.51(5).

two O atoms of the chelating hfac-ligand (Cu–O 1.9798 ± 0.0069 Å) and two N atoms of Py_3P. The axial positions are occupied by the third N atom of Py_3P and the O atom of second hfac-anion, the O3 atom of which remains noncoordinated. The Cu–N_{eq} distance is about 2.01 Å, whereas the Cu–N_{ax} bond length is significantly longer [2.2575(14) Å], indicating a Jahn–Teller axial elongation.[35] On the whole, these values are typical for the Cu^{II}–N_{Py} lengths.[36,37] The geometry of the [Cu(Py_3P)] cage of **3** deviates from the perfect C_3-symmetry; the dihedral angles between the pyridine plane are 55.66, 61.78 and 62.82°. The peculiarity of the packing of **3** is that the neighboring molecules in **3** are linked by F···F [$d_{F3\cdots F3'}$ = 2.759, $d_{F4\cdots F9}$ = 2.887, $d_{F2\cdots F8}$ = 2.923 Å], P···F [$d_{P1\cdots F1}$ = 3.267 Å], C_{hfac}···F [2.894, 3.071 Å], C_{Py}···F [2.928 Å], C_{Py}–H···F [2.483–2.620 Å] and C_{Py}–H···O_{hfac} [2.344, 2.640 Å] interactions to generate a 3D supramolecular network.

The structure of scorpionate **4** (Fig. 2) is almost perfectly consistent with that of **3** (overlay of these molecules is depicted in Fig. S1†). The major difference between them is the presence of an O atom of the P═O bond in **4**, the length of which [1.468(2) Å] is comparable with that in the free Py_3P = O [1.4792(11) Å].[38] Similarly, the Cu ion of **4** shows a typical Jahn–Teller axial elongation in its distorted octahedral geometry.

The asymmetric unit of **5** contains one noncoordinated hfac-anion and half of the cation $[Cu(Py_3P)_2]^{2+}$, where the Cu atom is located in an inversion center. The two Py_3P molecules are ligated to the Cu atom through six N atoms to form the bis-scorpionate structure that looks like a paddle-wheel (Fig. 3). Thus, the metal atom adopts a distorted octahedral geometry. It should be noted that in the CuN_6 unit of **5**, there are three pairs of unique Cu–N bonds with Cu–N distances of 2.2883(17) [Cu–N_{ax}], 2.1360(17) and 2.0192(14) Å [Cu–N_{eq}] that suggest a Jahn–Teller elongation along the *z*-axis. In contrast, in the related complexes, *e.g.* [Cu(Py_3P)$_2$]Br_2,[39] [Cu($MeCPy_3$)$_2$]I_2,[40] and [Cu($MeOCPy_3$)$_2$]$(OTf)_2$,[41] two short (*ca.* 2.0 Å) and four long (*ca.* 2.2 Å) Cu–N distances are observed. The O^1–C19–C18–C17–O^2 chain of the noncoordinated hfac-anions in **5** has a *syn–syn* conformation.

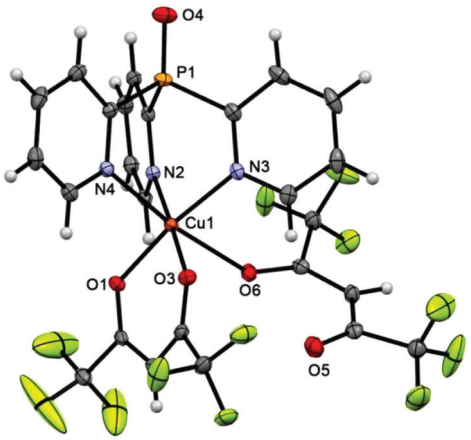

Fig. 2 Molecular structure of **4** (50% thermal ellipsoid). Selected bond lengths [Å] and angles [°]: Cu(1)–O(1) 1.9694(19), Cu(1)–O(2) 1.971(2), Cu(1)–O(6) 2.3988(19), Cu(1)–N(2) 2.023(2), Cu(1)–N(3) 2.029(2), Cu(1)–N(4) 2.345(2), P(1)–O(4) 1.468(2), O(1)–Cu(1)–N(3) 171.42(9), O(2)–Cu(1)–N(2) 177.79(9), N(4)–Cu(1)–O(6) 171.62(7).

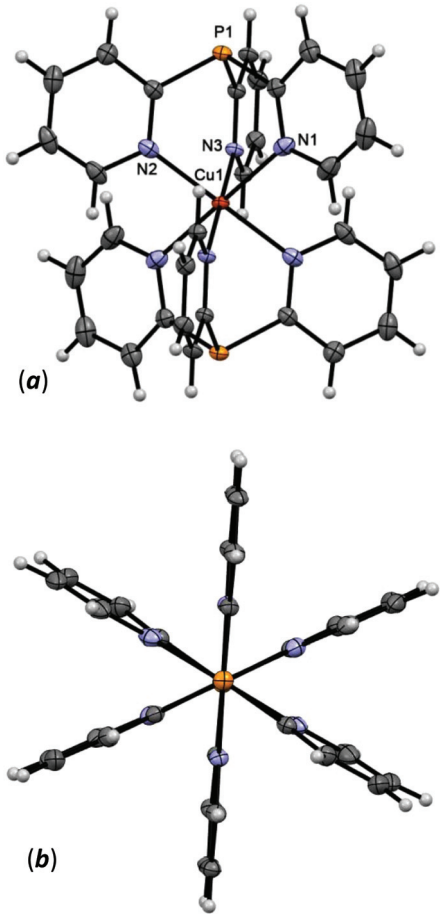

Fig. 3 Side-on (*a*) and top-down (*b*) views of structure of the $[Cu(Py_3P)_2]^{2+}$ cation of **5** (50% thermal ellipsoid). Selected bond lengths [Å] and angles [°]: Cu(1)–N(1) 2.2883(17), Cu(1)–N(2) 2.1360(17), Cu(1)–N(3) 2.0192(14), N(1)′–Cu(1)–N(1) 180.00(5), N(2)–Cu(1)–N(2)′ 180.00(5), N(3)–Cu(1)–N(3)′ 180.0, N(2)–Cu(1)–N(1) 90.75(6), N(3)–Cu(1)–N(2) 90.77(6).

The cationic parts of scorpionates **6** (Co^{II}) and **7** (Ni^{II}), $[M(Py_3P = O)(hfac)(H_2O)]^+$, are isostructural and have almost superimposable structures (see overlay of these molecules in Fig. S2†). As seen from Fig. 4 and 5, in both cations, Py_3P = O is bonded to a metal atom in a *N*,*N*′,*N*″-tripodal manner with three M–N bonds being nearly equal (average 2.126 Å). The *O*,*O*′-chelating hfac-anion and the oxygen atom of water completes the coordination sphere of the metal, representing a slightly distorted octahedron. The [M(N–C)$_3$P = O] cage has pseudo-C_3-symmetry with the dihedral angles between three mean Py cycles of 117.64–123.02° (for **6**) and 117.65–121.79° (for **7**). The M–O_{hfac} distances (*ca.* 2.052–2.114 Å) are longer than the M–O_{H_2O} bond (*ca.* 2.030 Å). The noncoordinated hfac-anion in **6** and **7** adopts a *syn–syn* conformation; it is linked with the coordinated water molecule through O_{H_2O}–H···O_{hfac}

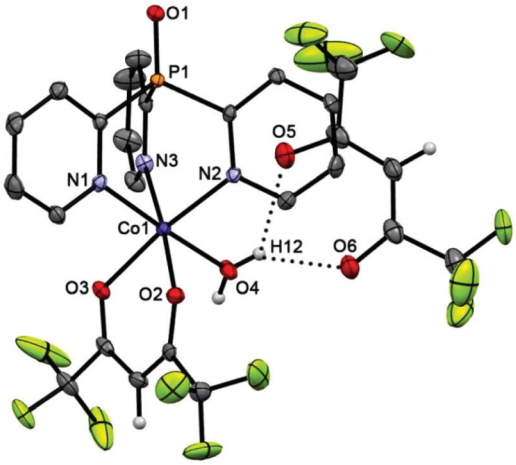

Fig. 4 Molecular structure of **6** (50% thermal ellipsoid). The pyridine hydrogen atoms are omitted for clarity. Selected bond lengths [Å] and angles [°]: Co(1)–O(4) 2.033(3), Co(1)–O(2) 2.070(3), Co(1)–O(3) 2.114(3), Co(1)–N(3) 2.116(3), Co(1)–N(2) 2.128(3), Co(1)–N(1) 2.133(3), P(1)–O(1) 1.479(3), H(12)–O(6) 2.0091(14), H(12)–O(5) 2.3020(12), O(4)–Co(1)–N(1) 176.86(13), O(3)–Co(1)–N(2) 173.44(12), O(2)–Co(1)–N(3) 175.47(13).

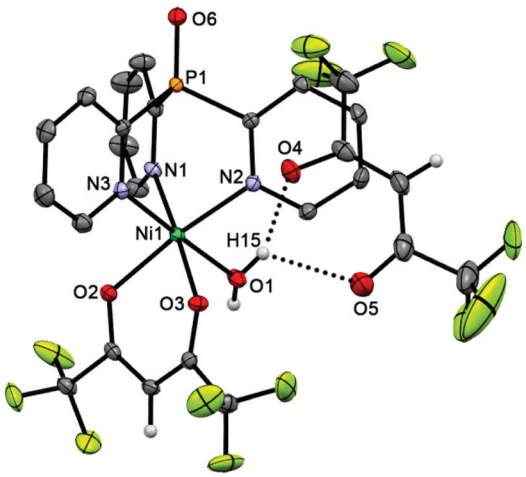

Fig. 5 Molecular structure of **7** (50% thermal ellipsoid). The pyridine hydrogen atoms are omitted for clarity. Selected bond lengths [Å] and angles [°]:]: Ni(1)–O(1) 2.028(2), Ni(1)–O(3) 2.052(2), Ni(1)–O(2) 2.061(2), Ni(1)–N(3) 2.068(3), Ni(1)–N(1) 2.069(3), Ni(1)–N(2) 2.081(2), P(1)–O(6) 1.478(2), H(15)–O(4) 2.0102(13), H(15)–O(5) 2.2952(13), O(1)–Ni(1)–N(3) 176.03(10), O(3)–Ni(1)–N(1) 176.32(9), O(2)–Ni(1)–N(2) 173.83(9).

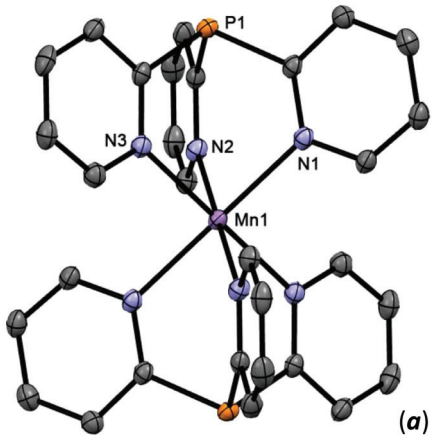

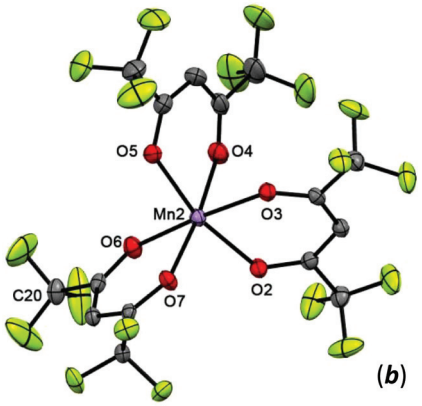

Fig. 6 The structure of cationic $[Mn(Py_3P)_2]^{2+}$ (*a*) and anionic $[Mn(hfac)_3]^-$ (*b*) of **8** (50% thermal ellipsoid). The pyridine hydrogen atoms are omitted for clarity. Selected bond lengths [Å] and angles [°]: Mn(1)–N(1) 2.2647(15), Mn(1)–N(2) 2.2453(15), Mn(1)–N(3) 2.2558(15), Mn(2)–O (3) 2.1714(13), Mn(2)–O(6) 2.1643(14), Mn(2)–O(5) 2.1488(14), Mn(2)–O(7) 2.1469(14), Mn(2)–O(4) 2.1372(14), Mn(2)–O(2) 2.1513(14), N(1)–Mn(1)–N(1)′ 180.0, N(2)′–Mn(1)–N(2) 180.0, N3–Mn(1)–N(3)′ 180.00(4), N(2)–Mn(1)–N(1) 86.79(5), O(6)–Mn(2)–O(3) 175.35(5), O(5)–Mn(2)–O(2) 166.70(5), O(4)–Mn(2)–O(7) 173.90(6).

hydrogen bonds (their parameters are given in the captions of Fig. 4 and 5).

Complex **8** crystallizes from acetone as the solvate **8**·2Me_2CO, which consists of a bis-scorpionate cation $[Mn(Py_3P)_2]^{2+}$ and two $[Mn(hfac)_3]_2^-$ anions (Δ- and Λ-enantiomers) per formula unit. In the cation, metal lies on a crystallographic inversion center (Fig. 6); it is coordinated in a tripodal manner by the three pyridine nitrogens of each ligand. The Mn(1) atom has a nearly perfect octahedral geometry with N–Mn–N angles of 180.00°. The Mn(1)–N distances (mean 2.255 Å) are comparable with those in $[MnCl_2(Py_3P)(OH_2)]$.[13] The $[Mn(hfac)_3]_2^-$ anions have a tris-chelate motif, with the Mn(2)–O distances varying from 2.1372(14) to 2.1714(13) Å. Analysis of bond angles within the MnO_6 polyhedron reveals that it can be best described as a twisted prism. On the whole, structures of the $[Mn(hfac)_3]_2^-$ anions in **8** are consistent with those in $PyH[Mn(hfac)_3]$[42] and $K[Mn(hfac)_3]$.[43]

2.3. Electrochemical properties

To elucidate the electrochemical features of the prepared complexes and possible products of their redox transformations, typically two successive cycles were measured. For the initial scan starting at 0.0 V (Ag/Ag^I), a potential was swept up to the positive direction. After two cycles were recorded, the experiment was repeated with the negative direction of the initial potential sweep. In all cases, voltammetry results at both Pt and glassy carbon (GC) electrodes were similar. The data for the first oxidation and first reduction peak potentials of the studied complexes have been summarized in the Table 1.

Table 1 The potentials of the first oxidation (E^{I}_{a}) and first reduction (E^{I}_{c}) peaks for complexes **3–8**

	GC electrode		Pt electrode	
Complex	E^{I}_{a}, V (Ag/Ag^{+})	E^{I}_{c}, V (Ag/Ag^{+})	E^{I}_{a}, V (Ag/Ag^{+})	E^{I}_{c}, V (Ag/Ag^{+})
3	0.987	−0.415	1.032	−0.483
4	0.980	−0.349	1.045	−0.371
5	0.958	−0.436	0.968	−0.378
6	0.969	—	1.057	—
7	0.942	—	0.972	—
8	0.94[a]	—	1.17[b]	−0.906

[a] Shoulder of the complex peak measured at the Nafion modified electrode (for details, see below). [b] Shoulder of the complex peak measured at the bare electrode.

Fig. 7 shows characteristic voltammograms of Py_3P = O based scorpionates **4**, **6** and **7**. The anodic current peaks at 0.95–1.00 V correspond to the first oxidation of the complexes. CV measured in the Py_3P = O solution of the same concentration demonstrates a weak quasi-reversible couple at the mentioned potentials, whereas the oxidation peaks of the studied complexes are electrochemically irreversible. It is worthwhile to note that neither the nature of the metal nor the type of ligand significantly influences the potential of the first oxidation peak. The peculiarity of Co^{II} complex (**6**) is the appearance of the second anodic oxidation peak at E = 1.414 V and the cathodic peak at E = 0.552 V on the reverse branch of CV. In our opinion, these peaks might be associated with the Co^{II}/Co^{III} redox transformations.

On the cathodic potential sweep in the solutions of Co^{II} (**6**) and Ni^{II} (**7**) complexes at potentials more negative than −0.5 V, the growth of a cathodic current was observed, although there were no cathodic peaks in the studied potential window. Even so, the products of cathodic reduction appeared in the solution and might be responsible for the anodic peak at −0.150/−0.140 V on the anodic branch of the CV.

The Cu^{II} scorpionate **4** demonstrated different cathodic behavior. Thus for its solution, a clear cathodic current peak was measured at −0.349 V. Some parts of the shape of this peak were quite complicated and probably corresponded to several overlapping redox reactions: one part was the same as for the above-mentioned reduction process of the Co^{II} and Ni^{II} complexes and was associated with the anodic peak at −0.140 V on the anodic branch of the CV, and another might have been associated to Cu^{II}/Cu^{I} reduction. This process is electrochemically irreversible, although the appearance of the broad anodic current peak at 0.317 V indicates an oxidation of a reduced complex on the reverse potential scan. Noteworthy, in this case, the cathodic scan was limited by potentials less negative than that needed for the first reduction, with the only anodic feature being an irreversible oxidation peak at the potential close to that of Co^{II} and Ni^{II} complexes.

The data shown in Fig. 8 allow one to estimate the influence of the ligands' nature and their number on the Cu^{II} complexes' voltammetry. The first oxidation current peaks appear at *ca.* 0.95 V for all of the studied substances, again evidencing that the nature of the ligand has a minor effect on the oxidation peak position. In contrast, the number of ligands coordinated to the metal strongly affects the value of the anodic current measured at the peak. Indeed, comparing the CV measured in the phosphine complexes' (**3** and **5**) solution of the same concentration, one could notice that for complex **5**, bearing two ligands, the oxidation current is two times higher than that for mono-scorpionate **3**.

In the series of additional experiments by varying the potential sweep rate, it has been found that the oxidation current peak value linearly depends on the square root of the sweep rate (see ESI† for corresponding data). Such a result suggests a diffusion control on the oxidation process and the absence of the hindrances from adsorption.[44] Taking into account the above-mentioned oxidation current ratio for mono- and bis-phosphine complexes, two assumptions can be deduced. First, the oxidation of complexes occurs presumably

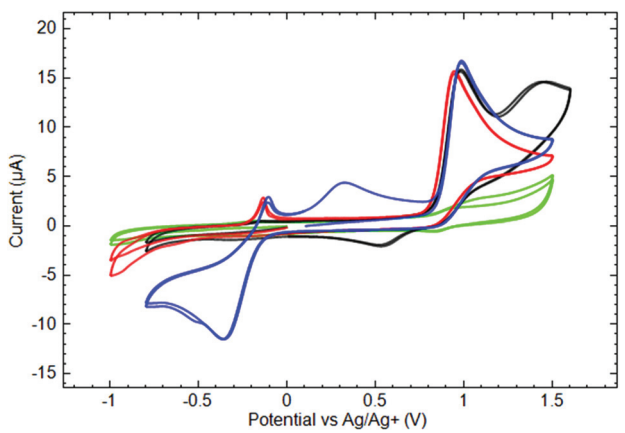

Fig. 7 Cyclic voltammograms of 10^{-3} M (—) **Py_3P = O**, (—) **4**, (—) **6**, and (—) **7** in 0.1 M TBAP acetonitrile solutions measured at the GC electrode (ν = 50 mV s^{-1}).

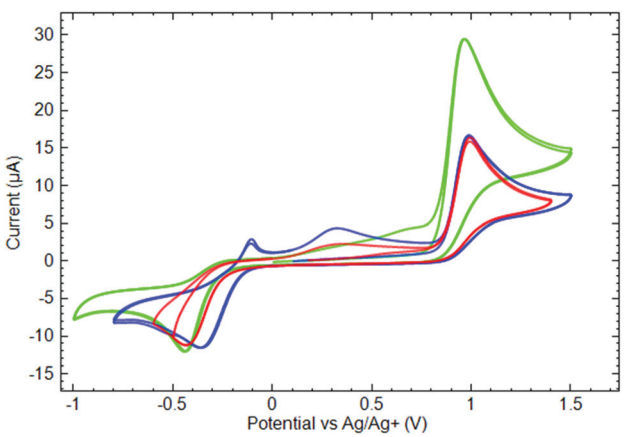

Fig. 8 Cyclic voltammograms of 10^{-3} M (—) **3**, (—) **4**, and (—) **5** in 0.1 M TBAP acetonitrile solutions measured at the GC electrode (ν = 50 mV s^{-1}).

through the ligands. Second, for bis-scorpionate complex **5**, both ligands are equally accessible for oxidation in the same potential scan.

On the cathodic branches of the CV (Fig. 8), there are irreversible peaks of cathodic current at −0.35/−0.45 V corresponding to the first reduction of the studied compounds. In contrast to the oxidation, the potentials of the reduction peak depend significantly on the type of ligand. In fact, for both phosphine complexes **3** and **5**, their reductions occur at potentials about 100 mV more negative than that for phosphine oxide **4**. Considering the oxygen atom in the phosphine oxide ligand as an electron withdrawing substituent, one could speculate on the role of such a center facilitating the reduction of the complex at less negative potentials. Despite the irreversibility of the cathodic peaks, the reduction products of all copper complexes undergo oxidation on the second anodic potential sweep, contributing to the growth of the anodic current in a potential region of 0.0/0.8 V.

As complex $[Mn(Py_3P)_2][Mn(hfac)_3]_2$ (**8**) contains Mn^{2+} ions both in the cationic and in the anionic parts, we attempted to separate their voltammetric responses. Because the Mn^{II} scorpionate composes the cationic part of the complex, CVs were measured at the Nafion coated GC electrode. According to Zook *et al.*,[45] Nafion behaves as a swelling membrane in acetonitrile in a similar way as in water solutions. The application of Nafion as a cation exchange membrane in non-aqueous solutions containing TBA^+ as a background cation is also known.[46] Voltammograms measured at the Nafion coated GC electrode remarkably differ from those measured at a bare GC (see ESI† for corresponding data). Fig. 9 shows CVs measured at the Nafion modified GC electrode in the **8** solution. At first glance, the anodic behavior of **8** differs significantly from all other studied complexes and demonstrates quasi-reversible characteristics of the first oxidation. However, in fact, the first oxidation current wave should be considered as a result of at least two overlapping processes. By varying the value limiting the anodic potential sweep, it was possible to confirm this suggestion. Indeed, until the anodic potential limit does not exceed 0.95 V, the oxidation remains irreversible and resembles other studied complexes. An inflection appears on the anodic branch of the voltammogram at the mentioned potential value and indicates the transition to the next redox process. Expanding the anodic potential limit above 0.95 V, leads to a registration of the cathodic current peak at 0.8 V on the reverse potential scan. Finally, at potentials more positive than 1.0 V, there is one more irreversible anodic current wave. Comparing the anodic behavior of **8** with other studied complexes, one can conclude that, in all cases, oxidation first involves the ligand moiety and demonstrates an irreversible characteristic. At the more positive potentials, the Mn site might be considered as an apparent target for oxidation.

CV measured at the bare Pt electrode in the **8** solution shows the irreversible cathodic current peak at −0.93 V and the anodic peak at 0.09 V on the reverse potential sweep. However, none of them are reproduced at the modified GC electrode. Indeed, in the studied potential region, there were no reduction peaks on the cathodic branch of the CV measured in the solution of **8** on the Nafion coated GC electrode, except for those assigned to the reduction of the products obtained in the anodic potential sweep. Such a difference can be attributed to the presence of Mn^{II} complexes both in cationic and in anionic parts of **8**.

2.4. Magnetic properties

Magnetic susceptibility data for complexes **3–8** were collected as a function of temperature from 2 to 300 K. Fig. 10 shows a representative plot of Cu^{II} complexes **3–5**. For **3**, the μ_{eff} value at 300 K is 1.91, which is in good agreement with the theoretical value ($1.86\mu_B$) for Cu^{II} ion, *i.e.* one paramagnetic centre with spin $S = 1/2$ and $g = 2.15$. The μ_{eff} value virtually does not change at lower temperatures down to 2 K. Thus, the characteristic of the $\mu_{eff}(T)$ dependence reveals the absence of significant exchange interactions and isolation of the paramagnetic

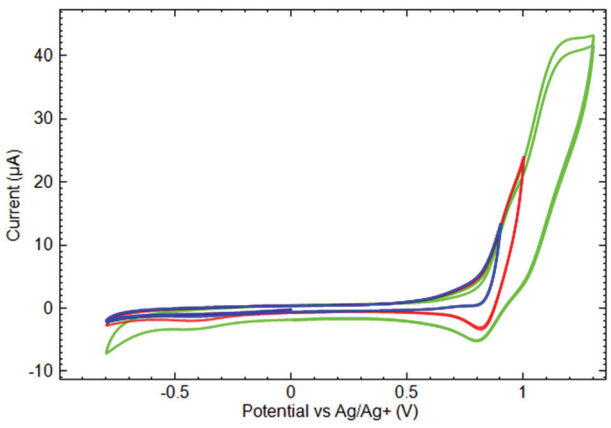

Fig. 9 Cyclic voltammograms of 10^{-3} M $[Mn(Py_3P)_2][Mn(hfac)_3]_2$ (**8**) in 0.1 M TBAP acetonitrile solution measured at a Nafion modified GC electrode by varying the positive sweep potential limit (ν = 50 mV s^{-1}).

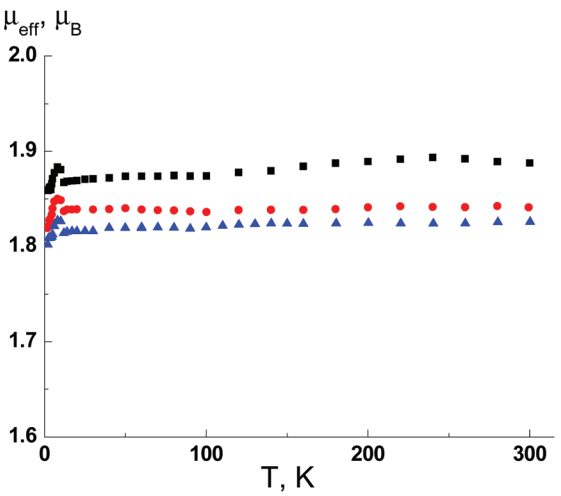

Fig. 10 The temperature dependence of the effective magnetic moment $\mu_{eff}(T)$ for **3** (■), **4** (●) and **5** (▲).

centres that is consistent with X-ray analysis data. As seen from Fig. 10, complexes **4** and **5** exhibit nearly the same magnetic behavior; their μ_{eff} values at 300 K are 1.84 and 1.83μ_B, respectively.

The temperature dependence μ_{eff} for Co^{II} complex (**6**) is presented in Fig. 11. At a lower temperature, μ_{eff} smoothly decreases from 4.67μ_B (300 K) to 3.46μ_B (2 K). The high temperature value of μ_{eff} is higher than the theoretical spin-only value for Co^{II} (S = 3/2, g = 2), which is consistent with the orbital contribution to the magnetic susceptibility, typical for Co^{II} ions in the octahedral environment and g-factors larger than 2. The μ_{eff} value at 300 K agrees well with typical values of 4.3–5.2μ_B for the Co^{II} ion. The decrease of μ_{eff} at lower temperatures is due to the spin–orbit interaction. The μ_{eff} value at low temperature is close to the theoretical spin-only value for the Co^{II} ion and indicates the absence of significant exchange interactions between the paramagnetic centres.

For Ni^{II} complex (**7**), the μ_{eff} value at 300 K is 3.07μ_B (Fig. 11), which agrees well with the theoretical value of 3.11μ_B for Ni^{II} with spin S = 1 and the g-factor of 2.2. Therefore, the dependence $\mu_{eff}(T)$ for **7** is quite similar to that for Cu^{II} complexes **3–5** (Fig. 10), showing the absence of significant exchange interactions between the paramagnetic centres.

For Mn^{II} complex (**8**), the μ_{eff} value at 300 K is 10.17μ_B and practically does not change when the temperature is lowered to 25 K but decreases to 9.77μ_B at 2 K. The μ_{eff} value for the temperature range of 300–25 K is in good agreement with the theoretical spin-only value, 10.25μ_B, for three non-interacting paramagnetic centers with S = 5/2 and g = 2 (Mn^{II} ions). The decreasing of μ_{eff} value below 25 K is due to weak antiferromagnetic exchange interactions.

Thus, magnetic measurements show that the paramagnetic nature of complexes **3–8** is defined by the M^{II} ions only; any exchange interactions between the paramagnetic centres are negligibly small. A magnetic saturation plays a role at low temperatures, where $\mu H \sim kT$ causes a small decrease of μ_{eff}. For comparison, the theoretical dependence of $\mu_{eff}(T)$, that takes into account the magnetic saturation, is shown in Fig. 12 by the solid line.

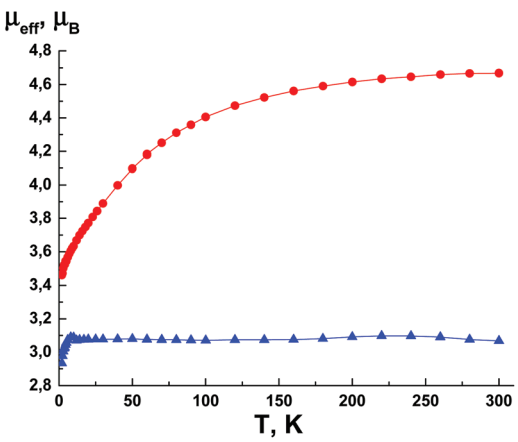

Fig. 11 The temperature dependence of the effective magnetic moment $\mu_{eff}(T)$ for **6** (●)and **7** (▲).

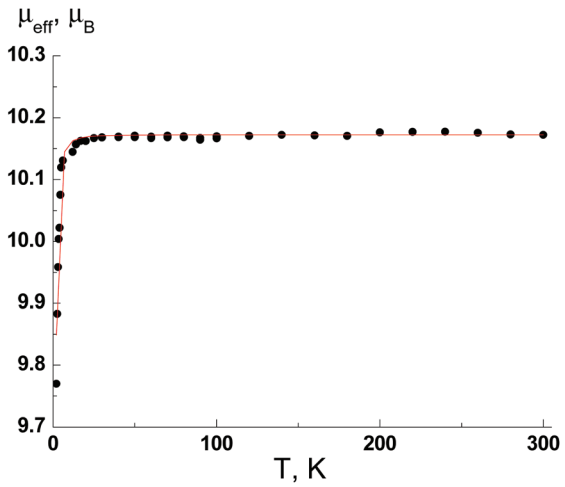

Fig. 12 The temperature dependence of the effective magnetic moment $\mu_{eff}(T)$ for **8**.

3. Conclusions

In summary, the coordination of tris(2-pyridyl)phosphine or its oxide toward $M(hfac)_2$ is accompanied by an unexpected replacement of the hfac-ligands by one or two tripodal ligands to afford mono- or bis-scorpionate complexes, respectively. The switching between the formation of one or another structure strongly depends on the nature of M^{II} and, in the case of $Cu(hfac)_2$, on the M/L ratio used. In the reaction with $Cu(hfac)_2$, the alteration of the Cu/L ratio from 1 : 1 to 1 : 2 alters the selectivity of the product formation from a mono-scorpionate to a bis-scorpionate complex, correspondingly. Moreover, Ni^{II} and Co^{II} hexafluoroacetylacetonates yield exceptional mono-scorpionates, even if the M/L ratio is 1 : 2. In contrast, $Mn(hfac)_2$, upon reacting with Py_3P, gives a complex composed of a bis-scorpionate cation $[Mn(Py_3P)_2]^{2+}$ and two $[Mn(hfac)_3]^-$ counterions.

CV measurements have shown that all synthesized compounds undergo irreversible oxidation at 0.95–1.00 V. The first electrochemical oxidation can be considered as an apparently ligand-centered process. Both the metal nature and the ligand type significantly influence the reduction of the complexes. The irreversibility of the voltammetric peaks suggests that an oxidation as well as a reduction of the studied complexes leads to significant structural changes or can be followed by some chemical transformations.

The magnetic measurements display that the coordination of tris(2-pyridyl)phosphine or its oxide to the M^{II} ion leads to the disappearance of the exchange interactions. As a result, paramagnetic M^{II} ions are well isolated magnetically from each other. Therefore, the tris(2-pyridyl)phosphine and its oxide are promising ligands in the design of single molecular (SMM) or single ion (SIM) magnets.

Keeping in mind the known data,[12,13] the synthesized complexes can be regarded as potential catalysts for organic transformations. Moreover, they are useful building blocks for the assembly of new heterometallic complexes, *e.g.* through coordination of the P atoms of **3**, **5** or **8** to the "soft" metal ions.

All of the results obtained contribute to the coordination chemistry of tripodal ligands and scorpionate complexes. The disclosed substitution of the anionic chelating ligand in the coordination sphere by the neutral tripodal ligand opens up new opportunities for the structure-oriented design of coordination compounds.

4. Experimental

4.1 General details

Solvents were purified following standard procedures prior to use. Tris(2-pyridyl)phosphine (**1**) was synthesized from red phosphorus and 2-bromopyridine according to the published method.[14] Phosphine oxide **2** was prepared by oxidation of **1** with H_2O_2 in water/acetone media. The $M(hfac)_2$ were prepared by the method of Bertrand and Kaplan.[47]

Elemental analyses were performed using a Flash EA 1112 CHNS analyzer. Melting points were determined with a Kofler micro hot stage. The IR spectra were recorded on a Varian 3100 FT-IR spectrometer with an ATR sample setting. XPRD analysis of samples **3–8** (see Fig. S20–S24†) was performed on a Shimadzu XRD-7000 diffractometer (Cu Kα radiation, Ni-filter, 5–35° 2θ range, 0.03° 2θ step, 5 s per point).

4.2 Electrochemistry

CVs have been recorded using Autolab PGSTAT 128N (The Netherlands) in MeCN solutions containing 0.1 M TBAP as a supporting electrolyte. Measurements were performed at room temperature in a convenient three electrode cell with either Pt (area 2.01 mm^2; BAS) or glassy carbon (GC, area 7.07 mm^2) working electrodes, Pt mesh counter electrode and a Ag/Ag^I reference electrode prepared with a BAS reference electrode kit filled with a CH_3CN solution containing 0.1 M TBAP and 0.01 M $AgNO_3$. The Ag/Ag^I reference electrode has been characterized in 0.1 M TBAP CH_3CN solution containing 1 mM ferrocene ($FeCp_2$). Both on Pt and on GC working electrodes, the $FeCp_2^+/FeCp_2$ couple shows $E_{1/2}$ = 0.120 V [estimated as $(E_{ap} - E_{cp})/2$] *vs.* a thus-prepared Ag/Ag^+ reference electrode. All potentials are given against this reference electrode. The concentrations of studied complexes were 1 mM, and a potential sweep rate (ν) was 50 mV s^{-1}. Prior to CV measurements, argon gas (99.99%) was passed through the solution in the cell for 10 min. For several CV experiments, the GC electrode modified by Nafion was prepared. Nafion solution (Aldrich) was coated onto the GC surface in a manner described earlier.[48] In order to equilibrate the Nafion film against the background electrolyte before CV measurement, the electrode was kept overnight in the MeCN 0.1 M TBAP solution.

4.3 Magnetochemistry

The magnetic susceptibility of the polycrystalline samples **3–8** was measured with a Quantum Design MPMSXL SQUID magnetometer in the temperature range of 2–300 K with a magnetic field of up to 5 kOe. None of the complexes exhibited any field dependence of molar magnetization at low temperatures. Diamagnetic corrections were made using the Pascal constants. The effective magnetic moment was calculated as $\mu_{eff}(T) = [(3k/N_A\mu_B{}^2)\chi T]^{1/2} \approx (8\chi T)^{1/2}$.

4.4 X-Ray crystallography

The single crystals of **3–7** and **8**·2Me_2CO were grown by slow liquid diffusion of hexane (*ca.* 7 mL) into an acetone or chloroform solution of these complexes (about 50 mg in 5 mL of the solvent). The mixture was allowed to stay at room temperature for a day. The precipitated crystals were collected, washed with a hexane/acetone (or chloroform) mixture and dried in air. Data were collected on a Bruker D8 Venture diffractometer with Mo Kα (λ = 0.71073 Å) radiation using the φ and ω scans. An empirical absorption correction was applied using the SADABS program.[49] The structures were solved and refined by direct methods using SHELX.[50] All non-hydrogen atoms were refined anisotropically using SHELX.[50] The coordinates of the hydrogen atoms were calculated from geometrical positions. The CF_3 groups within **3** (C^4) and **8** (C^{20}) were rotationally disordered, and two conformers were thus observed in the solid state.

CCDC 1431158 (**3**), 1431160 (**4**), 1431159 (**5**), 1033904 (**6**), 1036445 (**7**) and 1035512 (**8**) contain the supplementary crystallographic data for this article.

4.5 Synthetic procedures

[Cu(*N*,*N*′,*N*″-Py$_3$P)(*O*,*O*′-hfac)(*O*-hfac)] (3). To mixture of $[Cu(hfac)_2(H_2O)_2]$ (155 mg, 0.30 mmol) and tris(2-pyridyl)phosphine (80 mg, 0.30 mmol), $CHCl_3$ (6 mL) was added. The mixture was stirred at ambient temperature for 5 min to give an emerald-green solution, to which hexane (6 mL) was carefully added. The mixture was allowed to stay in an open vessel at room temperature. The resulting X-ray quality crystals were filtered off, washed with a hexane/$CHCl_3$ (1 : 1) mixture and dried in air. Yield: 197 mg (88%). Green crystals, mp 198–199 °C. IR (ATR): ν = 574 (m), 588 (m), 658 (s), 673 (m), 753 (m), 772 (s), 787 (s), 793 (s), 799 (m), 908 (w), 935 (w), 1004 (m), 1019 (m), 1059 (m), 1070 (m), 1127–1251 (vs, ν_{C-F} in CF_3), 1354 (w), 1428 and 1452 (m, $\nu_{C=C}$ in Py), 1530 and 1546 (m, $\nu_{C=N}$ in Py), 1587 (w), 1644 (s, $\nu_{C=O}$) 1669 (m, $\nu_{C=O}$), 3014 (w), 3066 (w) cm^{-1}. Anal. Calcd for $C_{25}H_{14}CuF_{12}N_3O_4P$ (742.90): C, 40.42; H, 1.90; N, 5.66. Found: C, 40.59; H, 1.89; N, 5.46.

[Cu(*N*,*N*′,*N*″-Py$_3$P = O)(*O*,*O*′-hfac)(*O*-hfac)] (**4**) was prepared from $[Cu(hfac)_2(H_2O)_2]$ (146 mg, 0.28 mmol) and tris(2-pyridyl) phosphine oxide (80 mg, 0.28 mmol) by a procedure similar to the one used for complex **3**. Yield: 172 mg (80%). Green crystals, mp 177–182 °C. IR (ATR): ν = 577 (m), 659 (s), 665 (s), 736 (m), 748 (s), 771 (m), 794 (m), 938 (w), 1007 (m), 1019 (m),

1048 (m), 1059 (m), 1088 (s), 1122–1253 (vs, ν_{C-F} in CF_3), 1433, 1439 and 1455 (m, $\nu_{C=C}$ in Py), 1487 (m), 1526 and 1548 (m, $\nu_{C=N}$ in Py), 1589 (w), 1646 (m, $\nu_{C=O}$), 2925–3264 br (w) cm^{-1}. Anal. Calcd for $C_{25}H_{14}CuF_{12}N_3O_5P$ (758.90): C, 39.57; H, 1.86; N, 5.54. Found: C, 39.42; H, 2.01; N, 5.47.

[Cu(*N*,*N*′,*N*″-Py$_3$P)$_2$](hfac)$_2$ (**5**) was prepared from $[Cu(hfac)_2(H_2O)_2]$ (73 mg, 0.14 mmol) and tris(2-pyridyl)phosphine oxide (80 mg, 0.28 mmol) by a procedure similar to the one used for complex **3** using MeCN as solvent. Yield: 112 mg (78%). Turquois crystals, mp 158–165 °C. IR (ATR): ν = 569 (m), 631 (w), 657 (s), 713 (m), 745 (m), 770 (s), 780 (s), 883 (w), 935 (m), 1004 (m), 1017 (m), 1061 (m), 1113–1242 (vs, ν_{C-F} in CF_3), 1278 (w), 1422 and 1455 (m, $\nu_{C=C}$ in Py), 1459 (m), 1524 and 1555 (m, $\nu_{C=N}$ in Py), 1570 (m), 1582 (m), 1669 (s, $\nu_{C=O}$), 3053 (w) cm^{-1}. Anal. Calcd for $C_{40}H_{26}CuF_{12}N_6O_4P_2$ (1008.15): C, 47.65; H, 2.60; N, 8.34. Found: C, 47.45; H, 2.51; N, 8.27.

[Co(*N*,*N*′,*N*″-Py$_3$P = O)(*O*,*O*′-hfac)(*O*-H$_2$O)](hfac) (**6**) was prepared from $[Co(hfac)_2(H_2O)_2]\cdot H_2O$ (150 mg, 0.28 mmol) and tris(2-pyridyl)phosphine oxide (80 mg, 0.28 mmol) using acetone as solvent. Yield: 187 mg (85%). Orange-red crystals, mp 127–130 °C. IR (ATR): ν = 570 (m), 574 (m), 583 (m), 594 (w), 618 (w), 659 (m), 665 (m), 674 (m), 737 (m), 750 (m), 772 (m), 796 (m), 937 (w), 1006 (w), 1018 (w), 1058 (w), 1072 (m), 1094 (m), 1147–1254 (vs, ν_{C-F} in CF_3), 1432 and 1455 (m, $\nu_{C=N}$ in Py), 1529 and 1547 (m, $\nu_{C=N}$ in Py), 1589 (w), 1646 and 1669 (s, $\nu_{C=O}$), 3018–3295 br (w) cm^{-1}. Anal. Calcd for $C_{25}H_{16}CoF_{12}N_3O_6P$ (772.30): C, 38.88; H, 2.09; N, 5.44. Found: C, 38.71; H, 2.15; N, 5.61.

[Ni(*N*,*N*′,*N*″-Py$_3$P = O)(*O*,*O*′-hfac)(*O*-H$_2$O)](hfac) (**7**) was prepared from $[Ni(hfac)_2(H_2O)_2]$ (145 mg, 0.28 mmol) and tris (2-pyridyl)phosphine oxide (80 mg, 0.28 mmol) by a procedure similar to the one used for complex **3**. Yield: 178 mg (81%). Pale green crystals, mp 151–153 °C. IR (ATR): ν = 576 (m), 587 (m), 659 (m), 670 (m), 738 (m), 750 (m), 772 (m), 795 (m), 938 (w), 1006 (w), 1018 (m), 1058 (m), 1072 (m), 1094 (m), 1099 (m), 1147–1254 (vs, ν_{C-F} in CF_3), 1433, 1439 and 1455 (m, $\nu_{C=N}$ in Py), 1486 (m), 1528 and 1547 (m, $\nu_{C=N}$ in Py), 1590 (w), 1647 and 1669 (s, $\nu_{C=O}$), 2952–3396 br (w) cm^{-1}. Anal. Calcd for $C_{25}H_{16}NiF_{12}N_3O_6P$ (772.06): C, 38.89; H, 2.09; N, 5.44. Found: C, 38.74; H, 2.18; N, 5.35.

[Mn(*N*,*N*′,*N*″-Py$_3$P)$_2$][Mn(hfac)$_3$]$_2$ (**8**) was prepared from $[Mn(hfac)_2(H_2O)_2]$ (172 mg, 0.34 mmol) and tris(2-pyridyl) phosphine (60 mg, 0.23 mmol) in MeCN (3 mL). Yield: 152 mg (69%). Yellow crystals, *ca.* 220 °C dec. IR (ATR): ν = 579 (s), 642 (m), 662 (s), 711 (w), 720 (w), 740 (m), 748 (m), 762 (m), 773 (s), 792 (s), 806 (m), 900 (w), 946 (m), 976 (w), 1010 (s), 1057 (s), 1091 (s), 1126–1246 (vs, ν_{C-F} in CF_3), 1341 (w), 1427 and 1459 (m, $\nu_{C=C}$ in Py), 1503 (s), 1524 and 1551 (m, $\nu_{C=N}$ in Py), 1584 (m), 1647 (s, $\nu_{C=O}$) cm^{-1}. Calcd for $C_{60}H_{30}F_{36}Mn_3N_6O_{12}P_2$ (1937.62): C, 37.19; H, 1.56; N, 4.34. Found: C, 37.04; H, 2.01; N, 4.10. The crystals of **8** were re-dissolved in acetone, and the yellow solution was layered with hexane. After several days, X-ray quality crystals of **8**·2Me$_2$CO (found: C, 38.41; H, 2.17; N, 4.17. Calcd: C, 38.60; H, 2.06; N, 4.09) were precipitated.

Acknowledgements

The authors acknowledge the financial support from the Russian Foundation for Basic Research (Grant 15-03-05591).

Notes and references

1 G. R. Newkome, *Chem. Rev.*, 1993, **93**, 2067–2089.
2 P. Espinet and K. Soulantica, *Coord. Chem. Rev.*, 1999, **193–195**, 499–556.
3 A. P. Sadimenko, *Adv. Heterocycl. Chem.*, 2011, **104**, 391–475.
4 R. J. Somerville, *Pyridyl phosphine complexes in the design of hydration catalysts*, PhD thesis, Victoria University of Wellington, 2015.
5 M. Wallesch, D. Volz, D. M. Zink, U. Schepers, M. Nieger, T. Baumann and S. Bräse, *Chem. – Eur. J.*, 2014, **20**, 6578–6590.
6 J. J. Liu, P. Galettis, A. Farr, L. Maharaj, H. Samarasinha, A. C. McGechan, B. C. Baguley, R. J. Bowen, S. J. Berners-Price and M. J. McKeage, *J. Inorg. Biochem.*, 2008, **102**, 303–310.
7 E. Drent, P. Arnoldy and P. H. M. Budzelaar, *J. Organomet. Chem.*, 1993, **455**, 247–253.
8 E. Drent, P. Arnoldy and P. H. M. Budzelaar, *J. Organomet. Chem.*, 1994, **475**, 57–63.
9 C.-Y. Kuo, Y.-S. Fuh, J.-Y. Shiue, S. J. Yu, G.-H. Lee and S.-M. Peng, *J. Organomet. Chem.*, 1999, **588**, 260–267.
10 H.-S. Wang and S. J. Yu, *Tetrahedron Lett.*, 2002, **43**, 1051–1055.
11 K. Kurtev, D. Ribola, R. A. Jones, D. J. Cole-Hamilton and G. Wilkinson, *J. Chem. Soc., Dalton Trans.*, 1980, 55–58.
12 A. Karam, R. Tenia, M. Martinez, F. López-Linares, C. Albano, A. Diaz-Barrios, Y. Sánchez, E. Catarí, E. Casas, S. Pekerar and A. Albornoz, *J. Mol. Catal. A: Chem.*, 2007, **265**, 127–132.
13 A. N. Kharat, B. T. Jahromi and A. Bakhoda, *Transition Met. Chem.*, 2012, **37**, 63–69.
14 B. A. Trofimov, A. V. Artem'ev, S. F. Malysheva, N. K. Gusarova, N. A. Belogorlova, A. O. Korocheva, Yu. V. Gatilov and V. I. Mamatyuk, *Tetrahedron Lett.*, 2012, **53**, 2424–2427.
15 A. Steiner and D. Stalke, *Organometallics*, 1995, **14**, 2422–2429.
16 C. J. L. Lock and M. A. Turner, *Acta Crystallogr., Sect. C: Cryst. Struct. Commun.*, 1987, **43**, 2096–2099.
17 G. Zhang, J. Zhao, G. Raudaschl-Sieber, E. Herdtweck and F. E. Kuhn, *Polyhedron*, 2002, **21**, 1737–1746.
18 S. A. S. Anaya, A. Hagenbach and U. Abram, *Polyhedron*, 2008, **27**, 3587–3592.
19 F.-W. Lee, M. C.-W. Chan, K.-K. Cheung and C.-M. Che, *J. Organomet. Chem.*, 1998, **563**, 191–200.
20 R. P. Shutte, S. J. Rettig, A. M. Joshi and B. R. James, *Inorg. Chem.*, 1997, **36**, 5809–5817.

21 A. Bakhoda, N. Safari, V. Amani, H. R. Khavasi and M. Gheidi, *Polyhedron*, 2011, **30**, 2950–2956.
22 A. V. Artem'ev, N. K. Gusarova, S. F. Malysheva, O. N. Kazheva, G. G. Alexandrov, O. A. Dyachenko and B. A. Trofimov, *Mendeleev Commun.*, 2012, **22**, 294–296.
23 K. R. Adam, P. A. Anderson, T. Astley, I. M. Atkinson, J. M. Charnock, C. D. Garner, J. M. Gulbis, T. W. Hambley, M. A. Hitchman, F. R. Keene and E. R. T. Tiekink, *J. Chem. Soc., Dalton Trans.*, 1997, 519–530.
24 T. Astley, M. A. Hitchman, F. R. Keene and E. R. Tiekink, *J. Chem. Soc., Dalton Trans.*, 1996, 1845–1851.
25 S. Hanf, R. Garcia-Rodriguez, A. D. Bond, E. Hey-Hawkins and D. S. Wright, *Dalton Trans.*, 2016, **45**, 276–283.
26 A. V. Artem'ev, N. K. Gusarova, V. A. Shagun, S. F. Malysheva, V. I. Smirnov, T. N. Borodina and B. A. Trofimov, *Polyhedron*, 2015, **90**, 1–6.
27 T. Gneuß, M. J. Leitl, L. H. Finger, N. Rau, H. Yersin and J. Sundermeyer, *Dalton Trans.*, 2015, **44**, 8506–8520.
28 A. V. Artem'ev, E. P. Doronina, M. I. Rakhmanova, A. O. Sutyrina, I. Yu. Bagryanskaya, P. M. Tolstoy, A. L. Gushchin, A. S. Mazur, N. K. Gusarova and B. A. Trofimov, *New J. Chem.*, 2016, **40**, 10028–10040.
29 A. G. Walden and A. J. M. Miller, *Chem. Sci.*, 2015, **6**, 2405–2410.
30 B. A. Trofimov, N. K. Gusarova, A. V. Artem'ev, S. F. Malysheva, N. A. Belogorlova, A. O. Korocheva, O. N. Kazheva, G. G. Alexandrov and O. A. Dyachenko, *Mendeleev Commun.*, 2012, **22**, 187–188.
31 M. D. Le Page, B. O. Patrick, S. J. Rettig and B. R. James, *Inorg. Chim. Acta*, 2015, **425**, 198–210.
32 D. T. Richens, *Chem. Rev.*, 2005, **105**, 1961–2002.
33 A. W. Maverick, F. R. Fronczek, E. F. Maverick, D. R. Billodeaux, Z. T. Cygan and R. A. Isovitsch, *Inorg. Chem.*, 2002, **41**, 6488–6492.
34 R. D. Shannon, *Acta Crystallogr., Sect. A: Cryst. Phys., Diffr., Theor. Gen. Cryst.*, 1976, **32**, 751–767.
35 M. A. Halcrow, *Chem. Soc. Rev.*, 2013, **42**, 1784–1795.
36 Md. B. Zaman, K. A. Udachin and J. A. Ripmeester, *CrystEngComm*, 2002, **4**, 613–617.
37 S. Delgado, A. Barrilero, A. Molina-Ontoria, M. E. Medina, C. J. Pastor, R. Jiménez-Aparicio and J. L. Priego, *Eur. J. Inorg. Chem.*, 2006, 2746–2759.
38 R. J. Bowen, M. A. Fernandes, P. W. Gitari and M. Layh, *Acta Crystallogr., Sect. C: Cryst. Struct. Commun.*, 2004, **C60**, o258–o260.
39 T. Astley, H. Headlam, M. A. Hitchman, F. R. Keene, J. Pilbrow, H. Stratemeier, E. R. T. Tiekink and Y. C. Zhong, *J. Chem. Soc., Dalton Trans.*, 1995, 3809–3818.
40 A. Santoro, C. Sambiagio, P. C. McGowan and M. A. Halcrow, *Dalton Trans.*, 2015, **44**, 1060–1069.
41 R. T. Jonas and T. D. P. Stack, *Inorg. Chem.*, 1998, **37**, 6615–6629.
42 E. Bouwman, K. G. Caulton, G. Christou, K. Folting, C. Gasser, D. N. Hendrickson, J. C. Huffman, E. B. Lobkovsky and J. D. Martin, *Inorg. Chem.*, 1993, **32**, 3463–3470.
43 S. I. Troyanov, O. Yu. Gorbenko and A. A. Bosak, *Polyhedron*, 1999, **18**, 3505–3509.
44 R. G. Compton and G. E. Banks, *Understanding Voltammetry*, Imperial College Press, London, 2nd edn, 2011, 429 p.
45 L. A. Zook and J. Leddy, *Anal. Chem.*, 1996, **68**, 3793–3796.
46 I. L. Escalante-Garcia, J. S. Wainright, L. T. Thompson and R. F. Savinell, *J. Electrochem. Soc.*, 2015, **162**, A363–A372.
47 J. A. Bertrand and R. I. Kaplan, *Inorg. Chem.*, 1966, **5**, 489–491.
48 A. V. Kashevskii, A. Y. Safronov and O. Ikeda, *J. Electroanal. Chem.*, 2001, **510**, 86–95.
49 SADABS, *v. 2008-1*, Bruker AXS, Madison, WI, USA, 2008.
50 G. M. Sheldrick, *SHELX-97, Programs for Crystal Structure Analysis (Release 97-2)*, University of Göttingen, Germany, 1997.